STUDY ON DISCRIMINANT METHODS OF WINTER PAVEMENT CONDITIONS BY IMAGE PROCESSING

Kiyoshi TAKEICHI[1], Yuya HIRAKOUCHI[1], Masaki KAMIURA[1], Jun UOZUMI[2] and Nobuyuki ITOH[3]

[1] Dept. of Civil Eng.,
Hokkaigakuen University
South-26, West-11, Chuo-ku,
Sapporo, Hokkaido, 064-0926, Japan
TEL : +81-11-841-1161
FAX : +81-11-551-2951
E-mail : takeichi@cvl.hokkai-s-u.ac.jp

[2] Dept. of Elect. & Inf. Eng.,
Hokkaigakuen University
South-26, West-11, Chuo-ku,
Sapporo, Hokkaido, 064-0926, Japan
TEL : +81-11-841-1161
FAX : +81-11-551-2951
E-mail : uozumi@eli.hokkai-s-u.ac.jp

[3] Hokkaido Development
Engineering Center
#11, South-1, East-2, Chuo-ku.
Sapporo, Hokkaido, 060-0051, Japan
TEL : +81-11-271-3028
FAX : +81-11-271-5115
E-mail : n-ito@decnet.or.jp

1. Introduction

Winter road conditions change substantially depending on weather and traffic conditions. For example, wet or slushy road surface conditions produced by daytime warmth or sunshine turn into ice crust or ice films at night. In road management, determining the timing and appropriate measures requires accurate assessment of road surface conditions.

There are concerns about using of only buried sensors to detect local road conditions. A method that can cover a wide area and accurately determine the condition of the entire surface is needed.

At present, an electric capacitance meter, an electric conductivity meter and a road surface reflectometer are used to measure moisture, including snow and ice, on road surfaces. A road surface sensor and a radiation thermometer are used to measure road surface temperature and atmospheric temperature.

In this study, we employed digital image processing as a discriminant method for wide areas and reported the results of the examination of digital images of various road surface conditions procured in the laboratory experiment and in the field.

2. Asphalt specimens in a single road surface condition

(1) Laboratory experiment

We used six specimens of porous asphalt concrete (30 cm × 30 cm × 5 cm), whose surface condition changes greatly according to road and weather conditions, for each road condition. As shown in Photo 1 (a - d), we chose four kinds of road surface conditions: dry, wet, ice-film and snow/ice. For ice-film, the surface is covered with a film of ice and there is a void filled with ice. Snow/ice is a condition with a void filled with snow and ice.

Images were taken with a digital camera (2.1 million pixels) in a low-temperature room with and without a flash at a height of 70, 100, 150 and 180 cm from the specimens.

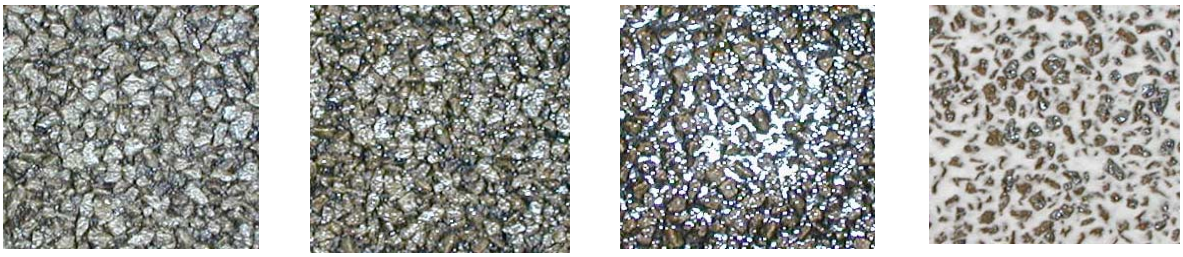

a. dry　b. wet　c. ice-film　d. snow/ice

Photo 1　Image of each road condition (taken at a height of 100 cm)

(2) Analysis method

a) Intensity and the number of pixels

Intensity (I) represents the intensity of light of image data stored on a personal computer. The gradation has a range of 256 values; higher intensity means brighter (whiter) and lower intensity means darker (blacker). An analysis was performed after cutting road surface images into 256×256 pixel frames.

b) Statistical parameters

The relationship between *I/Im* (the intensity *I* standardized by the mean intensity *Im*) and the probability density function $P_I(I)$ in equation (1) is shown in Figure 1 and Figure 2, with and without a flash, respectively. In both cases, dry and snow/ice conditions show similar distributions, while wet and ice-film conditions with a flash have a bimodal distribution with a peak at a high intensity like the snow/ice road surface condition. The reason is thought to be the reaction of the water film and the ice film to the flash.

The central moment M_k is expressed by equation (2), and from M_k (k = 2 - 4), contrast (V), skewness (Sk) and kurtosis (Ku) are expressed by (3), (4) and (5), respectively.

$$P_I(I) = \int_{-\infty}^{\infty} I(x)dx \quad (1)$$

$$\mathbf{M_k = \int_{-\infty}^{\infty} (I - Im)^k P_I(I) dI} \quad (2)$$

$$\mathbf{V = (M_2)^{\frac{1}{2}} / Im} \quad (3)$$

$$\mathbf{Sk = M_3 / (M_2)^{\frac{3}{2}}} \quad (4)$$

$$\mathbf{Ku = M_4 / (M_2)^2} \quad (5)$$

Contrast (V) is the degree of dispersion of the intensity distribution; a larger value indicates greater dispersion. Skewness measures the asymmetry of the data of a probability density function. The distribution is normal (symmetrical) when Sk = 0. When Sk < 0, the data are spread out more to the left of the mean, i.e., the left tail is longer; when Sk > 0, the right tail is longer. Kurtosis indicates the height of a probability density function, i.e., the degree of predominance of the intensity distribution. When the distribution is normal, Ku = 3; distributions have rapidly attenuating tails when Ku < 3, and slowly attenuating tails, Ku > 3.

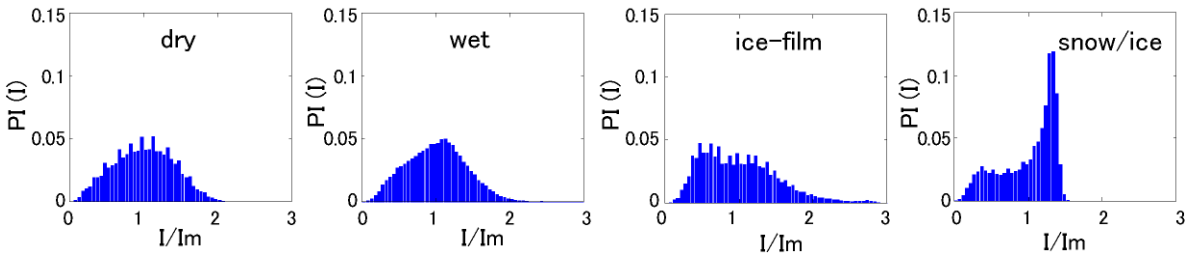

Figure 1 Intensity I/Im distribution without a flash

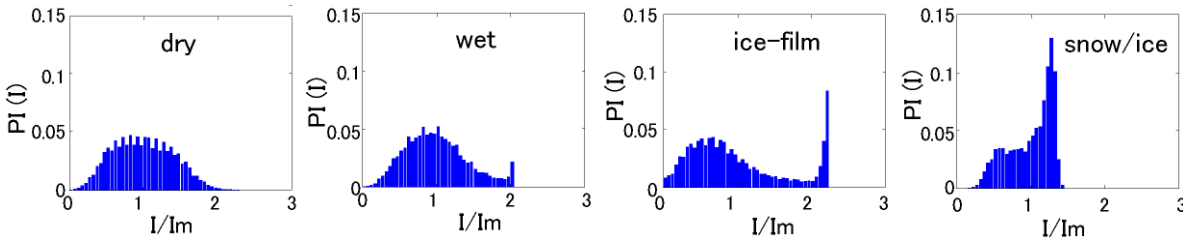

Figure 2 Intensity I/Im distribution with a flash

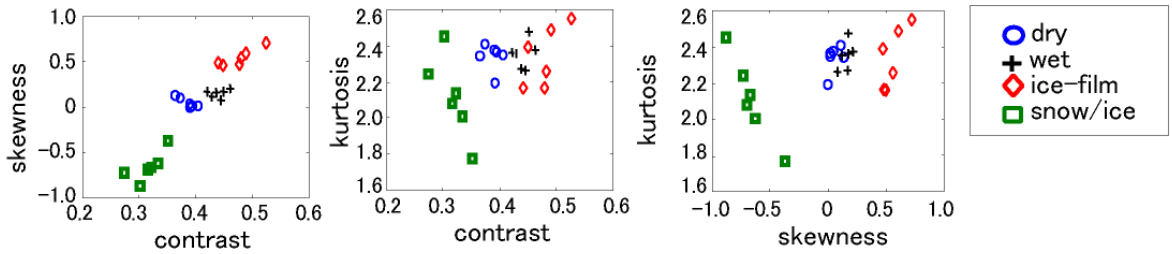

Figure 3 Relationships between contrast, skewness and kurtosis (h = 70 cm)

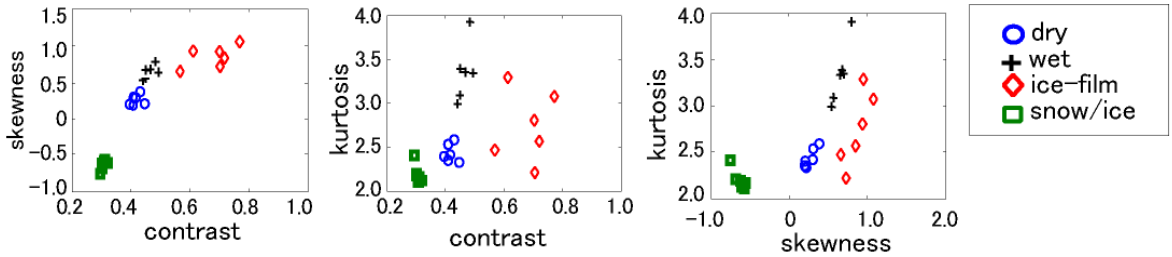

Figure 4 Relationships between contrast, skewness and kurtosis (h = 180 cm)

The results of the analysis of the relationships between contrast V, skewness Sk and kurtosis Ku are shown in Figure 3 and Figure 4 for when the camera height is 70 and 180 cm. A cluster of each road condition forms a little more clearly in the relationship between contrast and skewness than in other relationships. The upper limit of each parameter becomes slightly larger as the camera height increases (V: 0.53 → 0.78, Sk: 0.75 → 1.1, Ku: 2.58 → 3.90), a change which means that the distribution is spreading.

c) Autocorrelation function, $R_I(\Delta x, \Delta y)$

An autocorrelation function (equation (6)) shows the degree of correlation of the intensities of two points separated by distance (Δx, Δy). The points are pixels of 256 gradations. From the polar coordinate representation $R_I(r, \theta)$, with mean intensity *Im*, the angle-averaged autocorrelation function of the mean $R_I(r)$ is expressed by equation (7).

$$R_I(\Delta x,\Delta y)=\frac{1}{S}\iint_S\{I(x,y)-Im\}\{I(x+\Delta x,y+\Delta y)-Im\}dxdy \qquad (6)$$

$$R_I(r)=\frac{1}{2\pi}\int_0^{2\pi} R_I(r,\theta)d\theta \qquad (7)$$

Figure 5 shows the relationship between the autocorrelation function R_I and the pixels r for each road condition (h = 150 cm). The autocorrelation function tends to suddenly decline for each road condition with a difference of 5 or more pixels. This kind of difference according to road surface conditions is not clear.

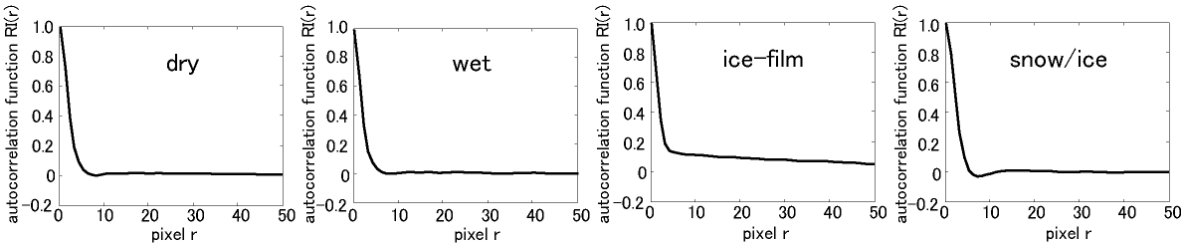

Figure 5 Relationship between autocorrelation function $R_I(r)$ and pixel r

d) Power spectrum, S_I (fx, fy)

Power spectrum S_I (fx, fy) shows the distribution of power of each frequency component with the assumption that a variable intensity wave form is the sum of a series of frequency components. From the polar coordinates representation $S_I(\rho, \phi)$ of S_I (fx, fy), the angle-averaged power spectrum $S_I(\rho)$ is obtained by equation (8).

$$S_I(\rho) = \frac{1}{2\pi}\int_0^{2\pi} S_I(\rho, \phi)\, d\rho \qquad (8)$$

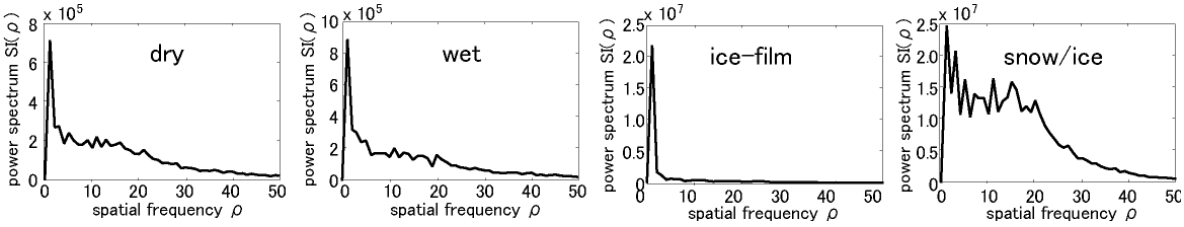

Figure 6 Relationship between power spectrum and spatial frequency

Figure 6 shows the relationship between spatial frequency ρ and power spectrum $S_I(\rho)$. For icy road surfaces, low frequency components are predominant and positional intensity fluctuations of road surfaces are small, whereas snow/ice road surfaces have many regions of low frequency components because of spotted road surfaces. Dry and wet road surfaces show a tendency in between these two, and frequency analysis reveals no clear difference between dry and wet road surfaces.

A mean value of $S_I(\rho)$ in the spatial frequency range $10 \leqq \rho \leqq 20$ is regarded as low frequency components (low freq.) and that in the range $40 \leqq \rho \leqq 50$ is regarded as high frequency components (high freq.). They are expressed by equations (9) and (10), respectively. Figure 7 shows the relationship between the low and high frequency components. Equation (11), a Fourier transform (FT), describes the relationship between the autocorrelation function ($R_I(\Delta x, \Delta y)$) and the power spectrum (S_I (fx, fy)).

$$\text{lowfreq.} = \frac{1}{11}\int_{20}^{10} S_I(\rho)\, d\rho \qquad (9)$$

$$\text{highfreq.} = \frac{1}{11}\int_{50}^{40} S_I(\rho)\, d\rho \qquad (10)$$

$$S_I(\text{fx}, \text{fy}) = FT[R_I(\Delta x, \Delta y)] \qquad (11)$$

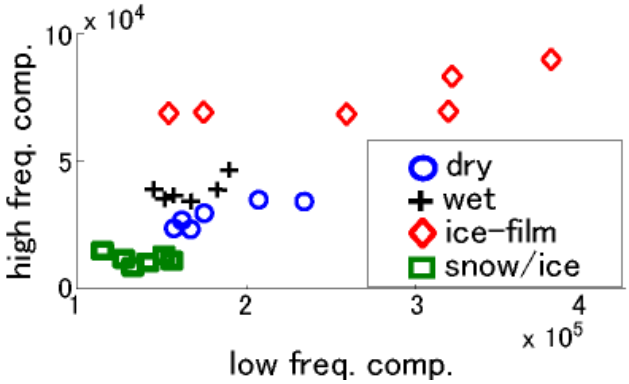

Figure 7 Relationship between low frequency component (low freq.) and high frequency component (high freq.)

3. Asphalt specimens in a complex road surface condition

(1) Analysis with parameters

Winter roads are prone to having fuzzy complex road surfaces rather than uniform ones. We examined complex road surface conditions, which are combinations of the individual road surface conditions mentioned before.

As shown in Photo 2, we made six specimens of road surfaces for each condition: dry+wet, dry+ice-film, dry+snow/ice, ice-film+wet, wet+snow/ice and snow/ice+ice-film.

A laboratory experiment used a similar method for single road surface conditions. Photo 2 shows photographs of complex road surfaces taken at a height of 180 cm. Figure 8 shows the relationships between V, Sk and Ku. A combination of each parameter discriminates between each road condition to some extent when taking into consideration that they are complex road surfaces. However, with adjacent clusters, discrimination based on these parameters is not always easy.

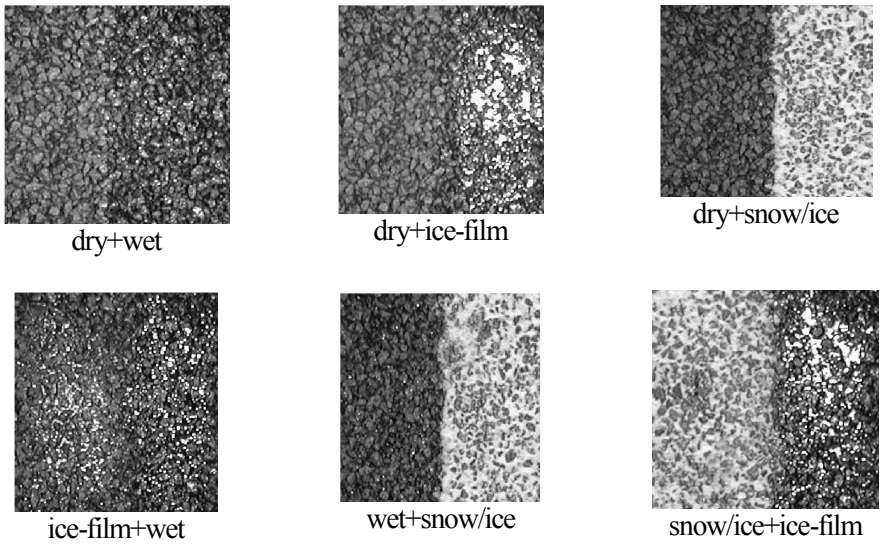

Photo 2 Images of complex road surface conditions

(2) Fuzzy inference

Applying fuzzy theory, we examined each road condition in terms of "certainty of occurrence" (goodness of fit) to make as objective a discrimination as possible.

In the analysis program, input variables in the antecedent part are V, Sk and Ku, and we call the goodness of fit of the occurrence of each road condition in the consequent part the rate of occurrence. Based on the results shown in Figure 8, it was determined that the range of the membership function for each complex road surface had seven grades, from negative large (N.L.) to positive large (P.L.), as shown in Table 1. Table 2 lists the rules for dividing the seven grades. Table 3 shows the results of the discrimination between road surfaces after using fuzzy theory to infer six images of each road condition.

Correctly predicted road surfaces are shown by half-tone dot meshing; falsely predicted road surfaces of the first rank are shown by double frames. The ranking of falsely predicted road surfaces is indicated with a 2), 3).

Seventy-eight percent (28/36×100) of the predictions were correct. Assuming that the first and second ranks of the rate of occurrence are included in the discrimination standard of the road management, prediction accuracy rises to 86% (31/36×100).

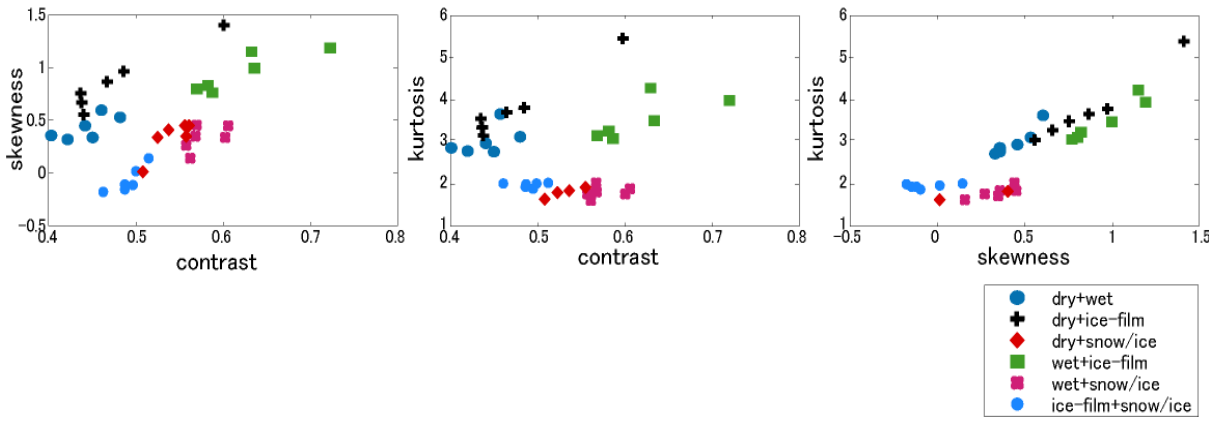

Figure 8 Relationships between contrast, skewness and kurtosis

Table 1 Range of the membership function for complex road surface conditions

	antecedent part						consequent part											
	contrast		skewness		kurtosis		dry+wet		dry+ice-film		dry+snow/ice		wet+ice-film		wet+snow/ice		ice-film+snow/ice	
	MIN	MAX	MIN	MAX	MIN	MAX	MIN	MAX	MIN	MAX	MIN	MAX	MIN	MAX	MIN	MAX	MIN	MAX
N.L	-∞	0.37	-∞	0.00	−∞	2.10	-0.17	0.17	-0.17	0.17	-0.17	0.17	-0.17	0.17	-0.17	0.17	-0.17	0.17
N.M	0.30	0.52	0.05	0.35	1.90	2.50	0.00	0.33	0.00	0.33	0.00	0.33	0.00	0.33	0.00	0.33	0.00	0.33
N.S	0.32	0.55	0.10	0.55	2.10	2.70	0.17	0.50	0.17	0.50	0.17	0.50	0.17	0.50	0.17	0.50	0.17	0.50
A.Z	0.37	0.61	0.20	0.50	2.50	3.15	0.33	0.67	0.33	0.67	0.33	0.67	0.33	0.67	0.33	0.67	0.33	0.67
P.S	0.40	0.63	0.25	0.85	2.75	3.40	0.50	0.82	0.50	0.82	0.50	0.82	0.50	0.82	0.50	0.82	0.50	0.82
P.M	0.45	0.68	0.35	1.00	2.90	3.50	0.67	1.00	0.67	1.00	0.67	1.00	0.67	1.00	0.67	1.00	0.67	1.00
P.L	0.59	∞	0.70	∞	3.10	3.70	0.82	1.17	0.82	1.17	0.82	1.17	0.82	1.17	0.82	1.17	0.82	1.17

Table 2 Rules set up for complex road surface conditions

antecedent part			consequent part						weight
contrast	skewness	kurtosis	dry+wet	dry+ice−film	dry+snow/ice	wet+ice-film	wet+snow/ice	ice-film+snow/ice	
N.M	N.M	N.S	P.S	A.Z	P.S	N.M	P.S	P.S	1.0
N.S	P.S	P.M	P.M	P.M	A.Z	P.S	N.S	A.Z	1.0
N.M	A.Z	P.S	P.L	P.S	A.Z	N.S	A.Z	A.Z	1.0
N.S	P.M	P.L	P.S	P.L	N.S	P.S	N.S	N.S	1.0
P.S	N.S	N.L	A.Z	N.S	P.L	N.S	P.M	P.M	1.0
P.M	N.S	N.L	A.Z	N.S	P.M	N.S	P.L	P.S	1.0
P.L	P.L	P.M	N.L	P.S	N.S	P.L	N.S	N.M	1.0
A.Z	N.L	N.L	A.Z	N.S	P.M	N.M	P.S	P.L	1.0

Table 3 Results of the inference of road surface discrimination by the fuzzy theory

actual road condition	road condition	No.	rate of occurrence of road condition					
			dry+wet	dry+ice-film	dry+snow/ice	wet+ice-film	wet+snow/ice	ice-film+snow/ice
	dry+wet	No. 1	0.827 2)	0.832	0.494	0.663	0.335	0.494
		No. 2	0.916	0.671	0.500	0.344	0.496	0.500
		No. 3	0.668 2)	0.920	0.332	0.668	0.332	0.332
		No. 4	0.865	0.654	0.518	0.317	0.516	0.518
		No. 5	0.850	0.648	0.523	0.311	0.522	0.523
		No. 6	0.896	0.693	0.500	0.397	0.474	0.500
	dry+ice-film	No. 1	0.670	0.920	0.330	0.670	0.330	0.330
		No. 2	0.670	0.931	0.336	0.667	0.333	0.336
		No. 3	0.626	0.861	0.331	0.689	0.330	0.313
		No. 4	0.670	0.920	0.330	0.670	0.330	0.330
		No. 5	0.743	0.865	0.409	0.667	0.333	0.409
		No. 6	0.830	0.833	0.497	0.666	0.334	0.497
	dry+snow/ice	No. 1	0.500	0.333	0.859	0.333	0.859	0.750
		No. 2	0.500	0.333	0.851	0.333	0.851	0.750
		No. 3	0.500	0.333	0.849	0.333	0.849	0.750
		No. 4	0.500	0.333	0.872	0.333	0.851	0.764
		No. 5	0.500	0.333	0.853 2)	0.333	0.870	0.740
		No. 6	0.500	0.330	0.835	0.330	0.835	0.750
	wet+ice-film	No. 1	0.222	0.687	0.333	0.865	0.330	0.191
		No. 2	0.080	0.670	0.330	0.920	0.330	0.170
		No. 3	0.080	0.670	0.330	0.920	0.330	0.170
		No. 4	0.750	0.835	0.415	0.670 3)	0.330	0.415
		No. 5	0.750	0.835	0.415	0.670 3)	0.330	0.415
		No. 6	0.750	0.835	0.415	0.670 3)	0.330	0.415
	wet+snow/ice	No. 1	0.500	0.333	0.845	0.333	0.878	0.727
		No. 2	0.500	0.333	0.834	0.333	0.905	0.687
		No. 3	0.500	0.333	0.849	0.333	0.849	0.750
		No. 4	0.500	0.333	0.856	0.333	0.863	0.745
		No. 5	0.500	0.333	0.834	0.333	0.916	0.684
		No. 6	0.500	0.333	0.838	0.333	0.838	0.750
	ice-film+ snow/ice	No. 1	0.596	0.426	0.744	0.239	0.744	0.739 3)
		No. 2	0.503	0.336	0.834	0.329	0.834	0.750 3)
		No. 3	0.500	0.333	0.833	0.172	0.667	0.947
		No. 4	0.500	0.333	0.833	0.172	0.667	0.937
		No. 5	0.500	0.333	0.833	0.172	0.667	0.948
		No. 6	0.500	0.333	0.833	0.172	0.667	0.948

: when correctly predicted
: when falsely predicted
2), 3) : ranking of the rate of occurrence when falsely predicted

4. Discrimination between road surfaces in the field

We took photographs of each road condition on municipal roads neighboring our university of Sapporo. Photographs were taken under natural light at a height of 70, 100, 150 and 200 cm. Photo 3 shows the various road surface conditions, including dry, wet, ice crust and compacted snow.

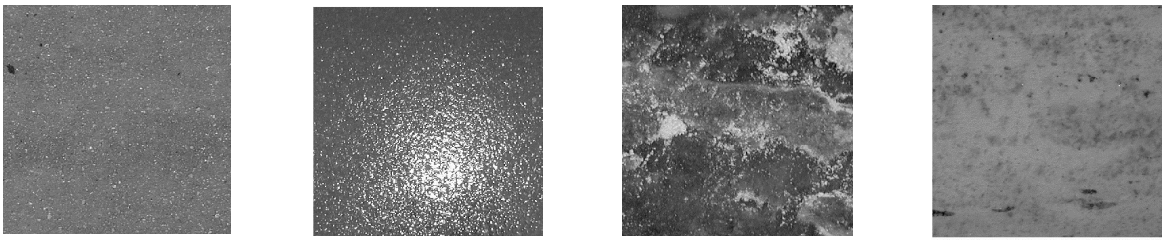

dry wet ice crust compacted snow

Photo 3 Image of each road condition on municipal roads

(1) Results of the analysis

Figure 9 shows the relationship between the probability density function P_I (I) and intensity (I/Im) of images of municipal road surfaces. The range of distribution was narrower than that of porous asphalt shown in Figures 1 and 2 for the reasons that the municipal roads were made with fine grained asphalt pavement, and that the snow and ice on the roads were uniform.

Figure 10 shows the relationships between contrast, skewness and kurtosis of the road surface images after analyzing six images of each road condition. Discrimination was easier than for the results of the laboratory experiment since clusters are formed for each road condition in combinations of each parameter.

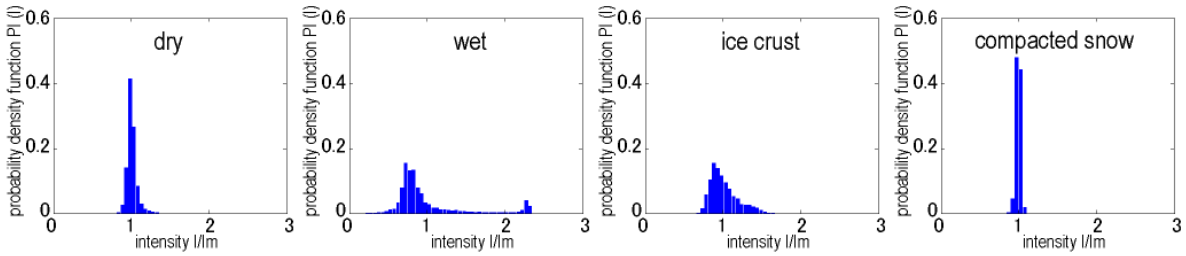

Figure 9 Relationship between probability density function PI (I) and intensity I/Im

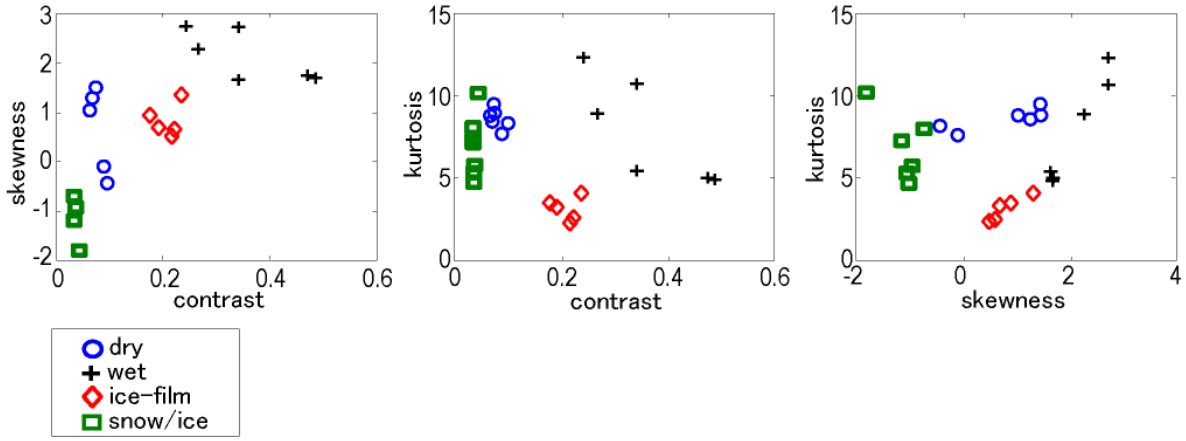

Figure 10 Relationships between contrast, skewness and kurtosis of road surface images of municipal roads

(2) Fuzzy inference

We also verified the accuracy of the discrimination by the fuzzy inference, based on the analyzed parameters. With the membership function and the rule setting thought in the same way as in the analysis of complex road surfaces, the results of the inference is shown in Table 4. When the results of the inference of each road condition was looked at with attention to the first rank of the rate of occurrence, actual road surfaces and inferred road surfaces all agreed with each other. This is partly because they were not in the complicated road surface condition.

Although verification in the field of a wider range of road surface conditions will be needed in the future, the discriminant method of road surfaces by the image analysis and the fuzzy inference is thought to be effective.

Table 4 Results of the discrimination between road conditions by the fuzzy inference

			rate of occurrence of road condition			
	road condition	No.	dry	wet	ice crust	compacted snow
actual road condition	dry	No. 1	0.889	0.441	0.697	0.754
		No. 2	0.885	0.440	0.700	0.753
		No. 3	0.891	0.441	0.697	0.754
		No. 4	0.885	0.440	0.700	0.755
		No. 5	0.901	0.441	0.696	0.754
		No. 6	0.894	0.441	0.697	0.754
	wet	No. 1	0.370	0.875	0.699	0.510
		No. 2	0.370	0.876	0.697	0.512
		No. 3	0.370	0.875	0.700	0.510
		No. 4	0.370	0.875	0.700	0.510
		No. 5	0.372	0.877	0.697	0.512
		No. 6	0.370	0.875	0.700	0.510
	ice crust	No. 1	0.541	0.596	0.920	0.754
		No. 2	0.542	0.596	0.933	0.754
		No. 3	0.540	0.598	0.920	0.752
		No. 4	0.540	0.595	0.920	0.755
		No. 5	0.540	0.598	0.920	0.752
		No. 6	0.540	0.595	0.920	0.755
	compacted snow	No. 1	0.542	0.441	0.535	0.948
		No. 2	0.540	0.440	0.535	0.948
		No. 3	0.542	0.441	0.535	0.948
		No. 4	0.540	0.440	0.533	0.948
		No. 5	0.542	0.441	0.534	0.948
		No. 6	0.540	0.441	0.535	0.946

5. Wavelet analysis

(1) Outline

Texture analysis using statistical parameters focusses on the intensity distribution of pixels in road surface images. The time (or space) domain is transformed to the frequency domain via Fourier transform to obtain the autocorrelation function and the power spectrum. An irregular intensity wave form is considered a series of frequency components.

However, temporal and spatial information is completely lost after the transform to the frequency domain. Consequently, spatial allocation and local existence of road surface conditions cannot be learned with this analysis. Commonly occurring examples of complex road surfaces would be a dry roadway surface with an ice crust surface on the shoulder and a road surface where longitudinal ruts have formed on ice crust.

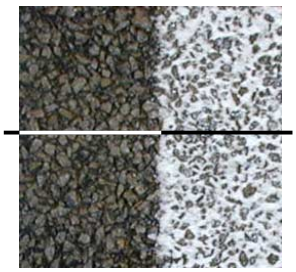

Photo 4 Surface of the specimen in the dry and snow/ice condition and the analysis line

In wavelet analysis, time and frequency analyses of signal intensity can be performed simultaneously. Not only frequency information but also time (positional) information can be obtained.

As a trial, we assumed a complex road surface with a dry surface on the left half and a snow/ice surface on the right half as shown in Photo 4, and examined the possibility of using wavelet analysis to discriminate between road surface conditions spatially.

(2) Wavelet transform

a) Continuous wavelet transform

If a wavelet function is expressed as $\psi(t)$, a base function $\psi_{a,b}(t)$ can be generated by translating $\psi(t)$ parallel to the t-axis (shift) and scaling it (dilation). $\psi_{a,b}(t)$ is expressed by equation (12).

$$\psi_{a,b}(t) = \frac{1}{\sqrt{a}}\psi\left(\frac{t-b}{a}\right) \qquad (12)$$

where a and b are parameters of scaling and parallel translation, respectively. The inner product of $\psi_{a,b}(t)$ and the signal f(t) gives the wavelet transform, and is expressed by equation (13). A wavelet development coefficient is a generated numerical value which represents the degree of similarity between the signal f(t) and the mother wavelet $\psi(t)$.

$$(W_{\psi}f)(b,a) = \frac{1}{\sqrt{a}}\int_{-\infty}^{\infty} f(t)\psi\left(\frac{t-b}{a}\right)dt \qquad (13)$$

In this study, we showed examinations of the results using Haar and Daubechies wavelets, the most basic of mother wavelets. Haar wavelet, the simplest mother wavelet, is expressed by equation (14).

$$\psi(t) = \begin{cases} 1\ (0 \leqq t < 1/2) \\ -1\ (1/2 \leqq t < 1) \\ 0\ (\text{otherwise}) \end{cases} \qquad (14)$$

b) Discrete wavelet transform

The discrete wavelet transform, which makes coordinates discrete, can be used for an effective time-frequency analysis of the signal. For the discrete wavelet, equation (12) is expressed by equation (15). In the equation, j is a level and k is an amount of shift. The signal f(t) is approximated by a linear combination of a scaling function $\varphi(t)$. An approximate function $f_0(t)$, a linear combination of $\varphi(t)$, is expressed by equation (16). The signal f(t) is expressed by the sum of linear combinations of wavelets and $\varphi(t)$ from level 1 to an arbitrary level.

$$\psi_{j,k}(t) = 2^{-\frac{j}{2}}\psi\left(2^{-j}t - k\right) \qquad (15)$$

$$f_0(t) = \sum_k s_k \varphi(t-k) \qquad (16)$$

S_k is a mean value of the signal f(t) in the section [k, k+1] and is expressed by equation (17).

$$s_k = \int_{-\infty}^{\infty} f(t)\overline{\varphi(t-k)}dt = \int_k^{k+1} f(t)dt \qquad (17)$$

With the shift and dilation of the integer of this scaling function thought of like wavelets, $\varphi_{j,k}$ is defined by equation (18). Also, an approximate function $f_j(t)$ of level j is expressed by equation (19), using $\varphi_{j,k}$.

$$\varphi_{j,k}(t) = 2^{-\frac{j}{2}}\varphi\left(2^{-j}t - k\right) \qquad (18)$$

$$f_j(t) = \sum_k s_k^{(j)}\varphi_{j,k}(t) \qquad (19)$$

$S_k^{(j)}$ is a scaling coefficient and obtained by the inner product of a scaling function $\varphi_{j,k}$.

$f_1(t)$ is a state lacking information from $f_0(t)$. This missing part $g_1(t)$ is a high frequency component. Accordingly, $f_0(t)$ is restored by equation (20) as a multiple resolution approximation (MRA).

$$f_0(t) = f_1(t) + g_1(t) \qquad (20)$$

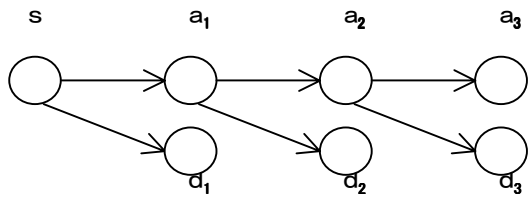

Figure 11 Decomposed model of the signal in the MRA

Figure 11 shows a decomposed model of the signal *s* used in this study. Low frequency component a_1 is obtained by removing high frequency component d_1 from s, and a_2 is obtained by removing d_2 from a_1. Conversely, the signal s is reconstructed by combining a_3, d_1, d_2 and d_3.

(3) Results of the analysis

Regarding the road surface in Photo 4 with a dry surface on the left half and a snow/ice surface on the right half, we transformed the wave form of the intensity distribution on the line crossing the photograph into a one-dimensional signal and analyzed its frequency distribution. Figure 12 shows an original signal of the one-dimensional frequency distribution crossing from the dry section to the snow/ice section. Figure 13 shows the results of the analyses using Haar and Daubechies (N = 10 wavelets).

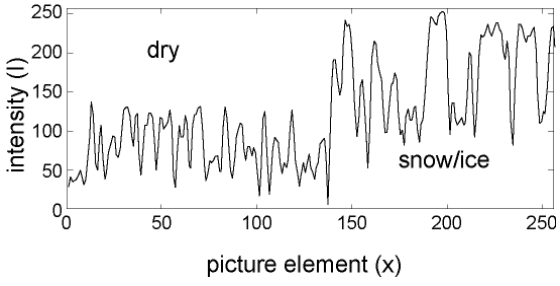

Figure 12 Original signal crossing between the dry section and the snow/ice section

a_3 is a low frequency wave form and d_3, d_2 and d_1 are high frequency wave components when level j = 3 - 1, respectively. Level j represents a scale of the mother wavelet. Level 2 is the level 1 scale doubled, and level 3 is level 1 scale tripled.

Looking at low frequency component a_3 in Figure 13, there is a remarkable difference in waveforms before and after the pixel count of around 150 for both of Haar and Daubechies, indicating a difference in road surface conditions.

However, because the frequency analysis of the relationship between frequency and a road surface condition corresponding to amplitude has not been made, the discrimination between road surface conditions cannot be made although information on the location is shown.

6. Conclusion

We obtained the following conclusions from the results of the laboratory and the on-site experiments on discriminant methods of winter road conditions based on image processing.

(1) The results of the laboratory and on-site experiments showed that three statistical parameters (contrast, skewness and kurtosis) were effective in discriminating between road surface texture of single road surface conditions. However, an autocorrelation function and a power spectrum generated by Fourier transform do not clearly show a difference in road conditions.

(2) The discrimination between complex road surfaces is sometimes not clear because clusters of parameters of each road surface are adjacent. However, by applying fuzzy theory, the percentage of true prediction reaches about 80 %.

(3) Although we performed a wavelet analysis to examine a method for discriminating between local parts of road surfaces, we could simply make the location of a different road surface condition clear. It is necessary to discriminate also between road surface conditions in the future, by giving a more detailed multiple resolution analysis of the original signal.

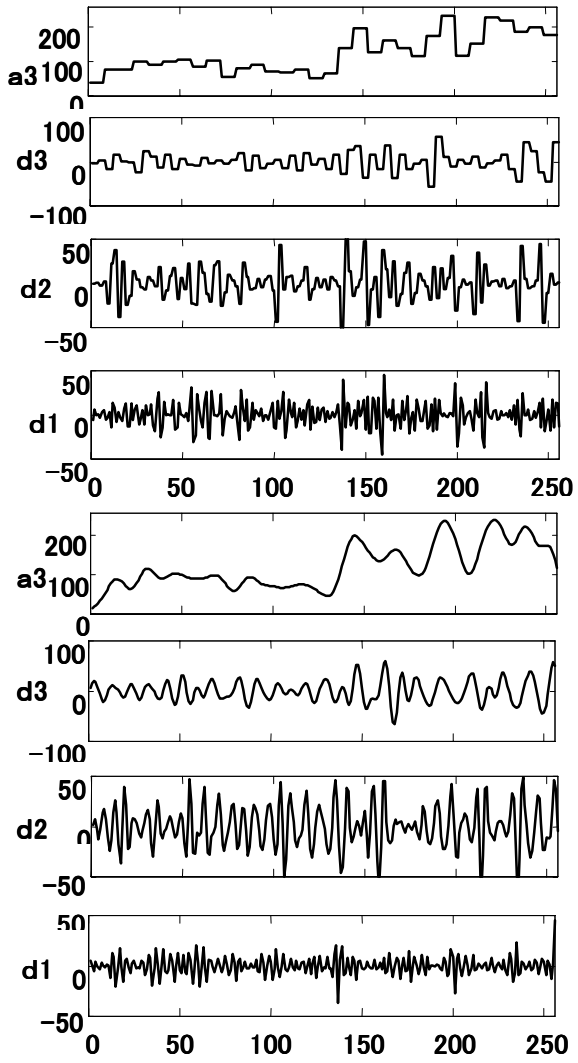

Figure 13 Results of the wavelet analyses using Haar (above), and Daubechies (N = 10) (below)

Reference

1) K. Hirakouchi, K. Takeichi: Discriminant Analysis of Complex Pavement Conditions by Digital Image Processing, Proc. of Japan Society of Civil Eng. (JSCE) Hokkaido, Vol.57, pp.712-715, 2001.2
2) J. Simawaki: Digital Image Processing (I) for Image Comprehension, Shocodo pulishing com., pp.60-94, 1991
3) Y. Yajima etc.: Statistics of Nature Science, Tokyo Uni. publication, pp.222-224, 1999
4) S. Nakamura: Digital Fourier Transform, Tokyo Denki Uni. Publication, pp48-87, 1999
5) H. Charles Romesburg: (Claster Analysis for Researchers), Robert E. Klieger publishing com. Inc., 1989
6) Y. Nakamura: Fuzzy Modeling, Ohm publishing com., pp.35-98, 1994
7) A. Kawamura: Recognition Methods of Pavement Roughness by Wavelet Function, 51Th Symposium Rep. V session of JSCE, pp.64-65, 1996
8) S. Sakakibara: Wavelet Beginner's Guide, Tokyo Denki Uni. publication, pp2-65, 1999
9) H. Nakano etc.: Signal and Image Processing by Wavelet, Kyoritsu publishing com., pp.17-63, 1999